Inorganic Chemistry

Article

pubs.acs.org/IC

Hexagonally Ordered $KLaF_4$ Host: Phase-Controlled Synthesis and Luminescence Studies

Shahzad Ahmad,[†] G. Vijaya Prakash,[‡] and R. Nagarajan*[,†]

[†]Materials Chemistry Group, Department of Chemistry, University of Delhi, Delhi 110007, India

[‡]Nanophotonics Laboratory, Department of Physics, Indian Institute of Technology, Delhi, New Delhi 110016, India

Supporting Information

ABSTRACT: Experiments resulting in the successful synthesis of hexagonally ordered $KLaF_4$ have been described for the first time. Syntheses from three different lanthanum precursors and KF under nonaqueous conditions and at atmospheric pressure are presented. The temperature, time of the fluorination reactions, and lanthanum precursor influenced the formation of hexagonal $KLaF_4$. While $La(O^iPr)_3$ and $La(acac)_3$ yielded hexagonal $KLaF_4$ by their reaction with KF in methanol at 65 °C, $LaCl_3$ favored only the formation of cubic $KLaF_4$ at 25 °C (room temperature). Size-induced phase transformation from cubic $KLaF_4$ to its hexagonal polymorph has been proposed for the reactions involving $La(acac)_3$ and $La(O^iPr)_3$ and KF. Rietveld refinement of the powder X-ray diffraction pattern of the hexagonally ordered $KLaF_4$ was successfully carried out in space group $P\bar{6}2m$ (No. 189) with lattice constants a = 6.5842(3) Å and c = 3.8165(3) Å. A relatively lower effective phonon energy of 262 cm^{-1} observed for the hexagonally ordered $KLaF_4$ (determined from its Raman spectrum) suggests its potential as a host for optically active elements with the possibility of minimized nonradiative processes. The hexagonal $KLaF_4$ sample was doped with Er^{3+} ion (3 mol %) and systematically investigated by diffuse reflectance, normal emission, and upconversion studies. Strong green emission ($^4S_{3/2}$, $^2H_{11/2} \rightarrow {}^4I_{15/2}$) has been observed upon 980 and 460 nm excitation. A highly transparent light-emitting polymer [poly(methyl methacrylate)] composite containing hexagonal $KLaF_4$:Er^{3+} phosphor has also been effectively demonstrated for many potential applications.

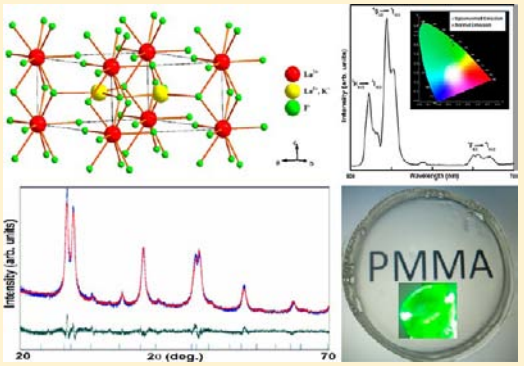

1. INTRODUCTION

Research on the lanthanide-doped upconversion (UC) energy systems continues to be a vibrant and growing interdisciplinary field, essentially in two directions.[1] One of them is tuning of the optical properties such as the high UC efficiency and emission profile in well-established energy UC systems, adopting different synthetic strategies, surface modification, and multicolor emission optimization. The other direction has been controlling the size, shape, and phase purity of the crystals of these systems from the applications point of view. In addition, the search for newer host fluoride lattices that are more effective for the UC process is also being pursued with the concomitant aim of understanding its role.[2]

The $NaLnF_4$ (Ln^{3+} = rare earth) system has attracted the attention of researchers as an efficient host matrix for green, red, and blue UC emission through appropriate doping.[3] The choice of fluorides as the host matrix for the UC studies has been justified because of its low phonon energy (preventing nonradiative relaxation) and multisite character of the host crystal lattice, i.e., occupation of the rare-earth active center in two or more nonequivalent crystallographic sites. Among the available synthetic strategies for solids, simple, robust, effective and convenient, energy-efficient solution-based techniques are being investigated for the synthesis of technologically important materials including nanophosphors.[4]

The critical role played by the size of the alkali-metal ions and the rare-earth ions in determining the structure type, lattice symmetry, and stoichiometry was exemplified by the research of Tyagi and co-workers,[5] in which Li_3ScF_6 (with Na_2GeF_6-type structure) was readily obtained at atmospheric pressure, while the scheelite structure type $LiScF_4$ was realized only at high pressures. Generally, $KREF_4$ has two polymorphs at room temperature and ambient pressure: orthorhombic and hexagonal, except in the case of $KLaF_4$ and $KCeF_4$, which possess a cubic phase.[6] Earlier, our group has reported efficient green UC emission by Er^{3+} doping[7] and strong red-emitting Eu^{3+}-doped $KLaF_4$,[8] a heavier analogue of the $NaYF_4$ system (crystallizing in the $Fm\bar{3}m$ cubic space group) by a green wet-chemical synthetic procedure. Following our studies, Liu et al.[9] have recently reported the controlled synthesis and optical properties of monodispersed nanoparticles of rare-earth-ion-doped cubic $KLaF_4$. Except for the identification of hexagonal $KLaF_4$ from the phase diagram of the KF−LaF_3 system by Zachariasen,[10] there are no further literature reports on the possible synthesis of this ordered lattice and it remains a challenge to date.

Received: July 18, 2012
Published: November 20, 2012

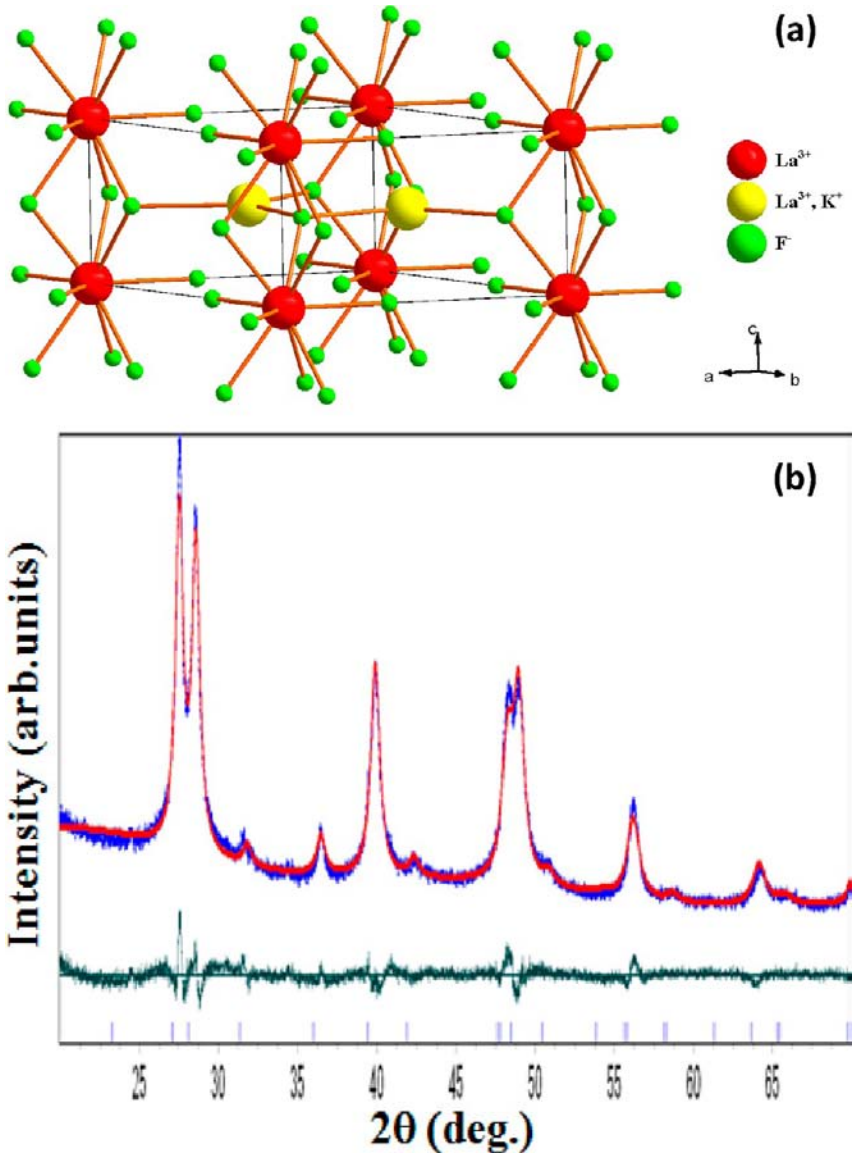

Figure 1. (a) Structure of hexagonal $KLaF_4$ using the *DIAMOND 3* program. (b) PXRD pattern of the hexagonal $KLaF_4$ sample [observed, calculated (profile matching), and difference profiles given respectively as blue, red, and olive-green lines and Bragg positions as blue vertical lines].

In the case of $NaYF_4$, it is observed that hexagonal ordering is thermodynamically more stable than its cubic form. Generally, the hexagonal phase has been stabilized by wet-chemical methods, with the hydrothermal method being the most investigated. Stabilization of the hexagonal phase of $NaYF_4$ has been achieved by the addition of excessive amounts of a fluoride source, conducting the reactions at high temperatures and by an aging process.[11] Usually, a chelating ligand [e.g., ethylenediaminetetraacetic acid (EDTA), cetyl trimethylammonium bromide, citrate, etc.] is reported to act as a phase controller, facilitating the slow and directed growth of the hexagonal phase. Optimization of various reaction parameters, such as the pH of the medium of growth and annealing temperature, was found to be a reason for the preferential synthesis of the hexagonal form without the presence of a cubic phase.[12] Recently, Chen et al.[13] developed a new strategy of synthesizing hexagonal $NaYF_4$ by doping-induced phase transition via a solvothermal method using Ti^{4+}, Zr^{4+}, and Ca^{2+} ions as dopants. Grzechnik et al.[14] studied the effect of high pressures (up to 11 GPa) at ambient temperature as well as at higher temperatures (up to 1100 °C) on the cubic-to-hexagonal phase transformation of $NaYF_4$.

In this paper, detailed investigations into the synthesis of hexagonally ordered $KLaF_4$ in pure form by the fluorination reaction of three different precursors of lanthanum and KF in a nonaqueous medium and at atmospheric pressures are described. It has been observed that the preferred phase formation, purity, and size of $KLaF_4$ crystals are sensitive to the starting lanthanum precursor, reaction time, and temperature. The phonon energy of this host matrix has also been determined from the Lorentzian fitting of its Raman spectrum for the first time. Doping of this host lattice with the optically active Er^{3+} ion was carried out to functionalize it to be a robust fluorescence host system.

2. EXPERIMENTAL SECTION

A series of experiments were conducted by reacting $LaCl_3$ (Sigma Aldrich 99.9%, 0.2452 g, 1 mol), La $(acac)_3 \cdot xH_2O$ (Sigma Aldrich, 0.4362 g, 1 mol), and $La(O^iPr)_3$ (Sigma Aldrich, 0.3162 g, 1 mol) with KF (Merck, GR 0.2324 g, 4 mol). Methanol was employed as the

dx.doi.org/10.1021/ic301566e | *Inorg. Chem.* 2012, 51, 12748−12754

solvent medium for the reactions involving $LaCl_3$ and $La(acac)_3$. A mixed-solvent system of isopropyl alcohol and methanol was used for the reaction of $La(O^iPr)_3$ and KF. Typically, the reactants were dissolved in 20 mL of the solvent. The solution containing the lanthanum ion was added dropwise under constant stirring to a KF solution. For doping studies, $Er(acac)_3$, prepared from $ErCl_3·6H_2O$ (Sigma-Aldrich, 99.9%), was used.[15]

The powder X-ray diffraction (PXRD) patterns were collected using a Bruker Discover D8 high-resolution diffractometer employing Cu Kα radiation (λ = 1.5418 Å) over the range of 2θ = 10–70°. The structure refinement of the PXRD data was carried out by the Rietveld method using *TOPAS3* software.[16] The thermogravimetric analysis of the samples was carried out using Perkin Elmer Diamond TG/DTA system from room temperature to 500 °C at a heating rate of 10 °C min^{-1}. The high-resolution transmission electron microscopy (HRTEM) images of the samples were collected using a Philips Tecnai G^2 30 transmission electron microscope operating at an accelerating voltage of 300 kV. A Raman spectrum of the sample, in compact form, was collected using a Renishaw spectrophotometer equipped with a microscope and an Ar^+ laser (λ = 785 nm, 10 mW). Diffuse-reflectance spectra of the samples were obtained using a Perkin-Elmer Lambda-35 UV–vis spectrophotometer attached to an integrating sphere. $BaSO_4$ was used as the reference for these measurements. The conventional excitation and emission spectral measurements of the sample [dispersed in water (1 wt %)] was carried out using Horiba Jobin Yvon Fluorolog modular spectrofluorimeter at room temperature employing a continuous-wave xenon lamp source. The steady-state and time-resolved UC emission measurements in solid form were performed employing a 980 nm diode laser as the excitation source using the setup as shown in ref 7. The emission light was dispersed into a monochromator (Acton SP 2300) coupled to a photomultiplier tube (calibrated with mercury emission) through an appropriate lens system. For time-resolved emission, a mechanical chopper (12 Hz), a lock-in amplifier, and a digital storage oscilloscope were used to record the transient response.

3. RESULTS AND DISCUSSION

3.1. Synthesis, Structure, and Morphology. In order to establish the optimal conditions for the synthesis of pure hexagonal $KLaF_4$, a series of reactions in a nonaqueous medium were carried out by systematically varying the lanthanum precursor, utilizing KF as the fluorinating and structure-directing agent. The addition of a lanthanum precursor solution (in methanol or isopropyl alcohol) to KF (in methanol) at room temperature resulted in a white suspension. Two different approaches were followed after this step. In one, the reaction was continued at room temperature under constant stirring for ~12 h, and in the other, the suspension was aged at 65 °C for ~12 h.

The reaction between $LaCl_3$ and KF, driven by salt elimination, was very fast at room temperature, and the PXRD of the product contained reflections pertaining to KCl, cubic $KLaF_4$, and LaF_3. After repeated washing with methanol, the complete removal of KCl occurred, resulting in cubic $KLaF_4$ (as the major phase) and LaF_3 (as the minor phase). The aging reaction performed at 65 °C for 12 h yielded only LaF_3. Relevant data have been provided in Figure S1 in the

Table 1. Crystallographic Data of Hexagonal $KLaF_4$

formula	$(KLaF_4)_{1.5}$
cryst syst	hexagonal
space group	$P\bar{6}2m$ (No. 189)
a (Å)	6.5842(3)
c (Å)	3.8165(3)
V (Å^3)	143.289(2)
Z	1
ρ_{calc} (g/cm^3)	4.415(5)
R_{exp} (%)	4.38
R_p (%)	5.38
R_{wp} (%)	6.67
GOF (S)	1.5
step size (deg)/step time (s/step)	0.01/1.5
no. of data points (2θ = 20–70°)	5000
no. of param	21
no. of restraints	2
temperature (K)	298

Table 2. Refined Positional Parameters after the Final Cycle of Refinement[a]

atom	site	SOF	x	y	z	B_{eq}
La1	1a	1.0	0.0	0.0	0.0	1.0
K1/La2	2d	0.75/0.25	0.3333	0.6667	0.5	1.0
F1	3g	1.0	0.6288(2)	0.0	0.0	1.0
F2	3f	1.0	0.2152(3)	0.5	0.5	1.0

[a]Refined unit cell parameters a = 6.5842(3) Å and c = 3.1865(3) Å.

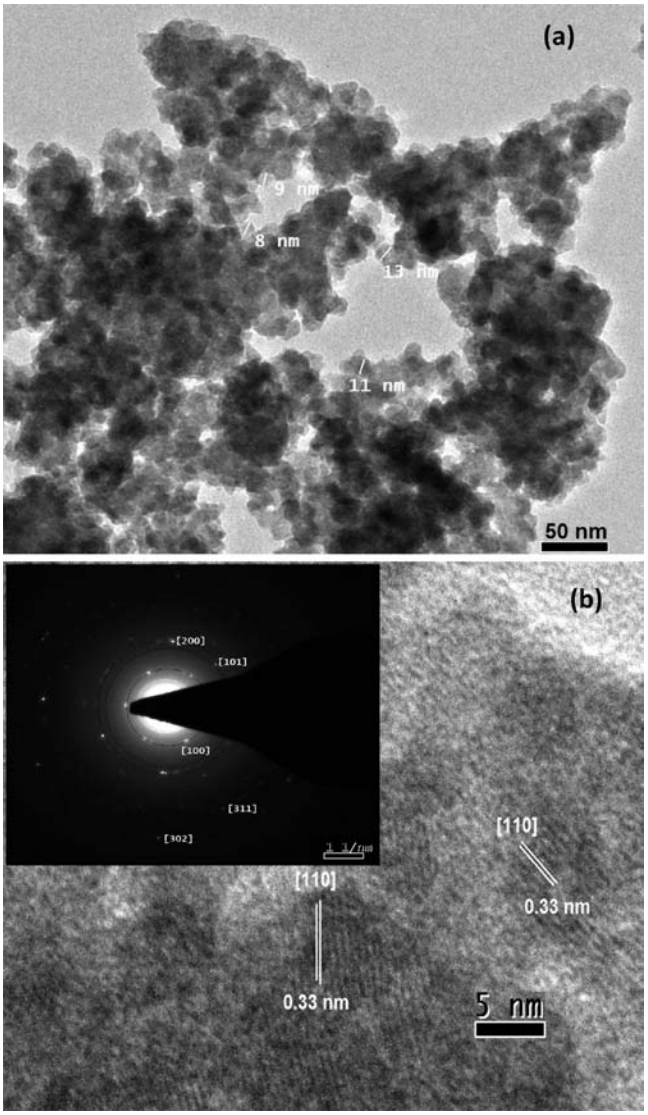

Figure 2. (a) TEM image of the hexagonal $KLaF_4$ sample. (b) HR-TEM image of the hexagonal $KLaF_4$ sample. A SAED pattern of the crystal is shown in the inset.

dx.doi.org/10.1021/ic301566e | *Inorg. Chem.* 2012, 51, 12748–12754

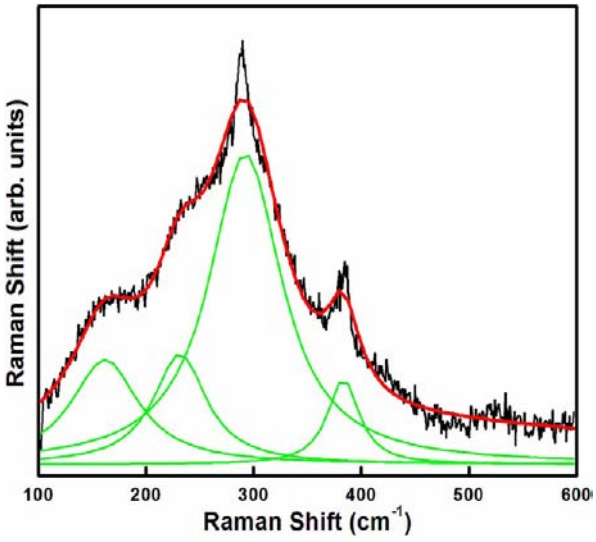

Figure 3. Room temperature Raman spectrum of the hexagonal $KLaF_4$ sample.

Supporting Information (SI). Taking the lead from the fact that those ligands capable of expanding the coordination number of the metal ions (such as EDTA) favor the formation of hexagonally ordered $NaYF_4$, two different lanthanum precursors, viz., $La(acac)_3$ and $La(O^iPr)_3$, were reacted with KF at room temperature as well as at 65 °C. The reactions were not as rapid as in the case of $LaCl_3$. The high chelate constants and the polymeric nature of these precursors might have influenced the slow formation kinetics of the final products. While the products from the room temperature reactions of $La(acac)_3$ and $La(O^iPr)_3$ were identified to be the cubic $KLaF_4$ phase from their PXRD patterns, the aging reactions performed at 65 °C using these two lanthanum precursors yielded products whose PXRD patterns matched well with the hexagonal form of $KLaF_4$ (JCPDS file no. 75-1927 and Figure S2 in the SI). The reflections in the PXRD pattern of hexagonal $KLaF_4$ were sharp and intense, implying good crystallinity. No other crystalline byproducts were observed in these sets of reactions. The reproducibility as well as the yield of hexagonal $KLaF_4$ from the reaction involving $La(O^iPr)_3$ was quite high compared to that of $La(acac)_3$, indicating the subtle difference in their behavior as precursors in the fluorination reaction. This might again be related to the different chelate constants of the ligands as well as the difference in the vapor pressures of $La(acac)_3$ and $La(O^iPr)_3$ when subjected to aging at 65 °C.

It is interesting to analyze these results to find the key factors responsible for this phase transformation from cubic to hexagonal in $KLaF_4$. First, the observation of LaF_3 being the only crystalline product for the reaction between $LaCl_3$ and KF conducted at 65 °C suggested that the cubic $KLaF_4$ phase was a kinetically stable one, undergoing dissociation to the thermodynamically more stable LaF_3. Additionally, the formation of cubic $KLaF_4$ at room temperature and hexagonal $KLaF_4$ at 65 °C from the other precursors indicated that the temperature of the reaction might be one of the factors inducing the transformation. To verify this, solid cubic $KLaF_4$ obtained using $La(acac)_3$ was subjected to thermogravimetric/differential thermal analysis (TG-DTA) in which no exothermic signal (usually observed for the cubic−hexagonal phase transition in $NaYF_4$) was observed until 500 °C, signifying the absence of a solid−solid phase transition (Figure S3 in the

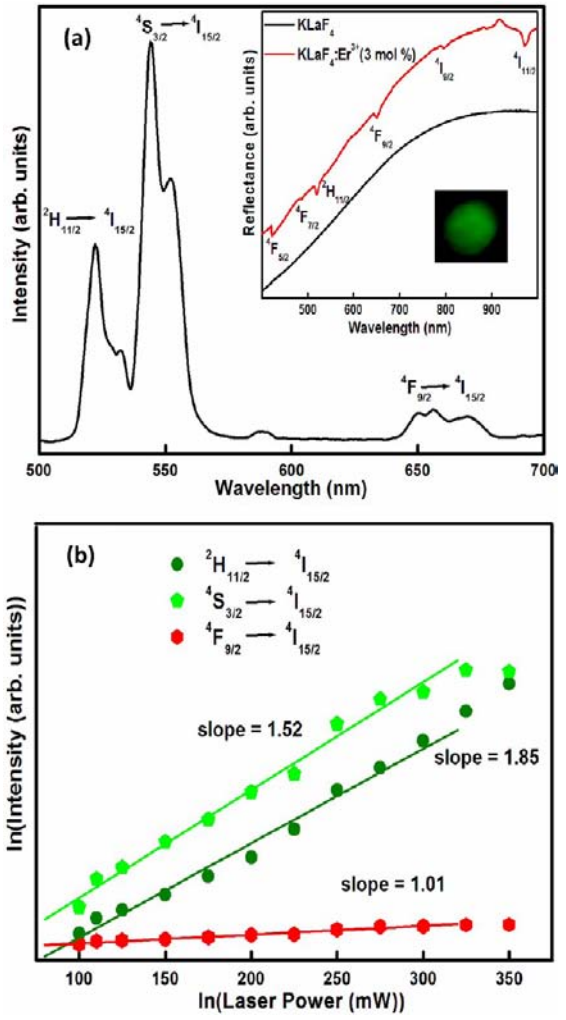

Figure 4. (a) UC spectra of the hexagonal $KLaF_4$:Er^{3+} (3 mol %) sample excited with a 980 nm laser at 150 mW power. UV−visible diffuse-reflectance spectra of undoped and 3 mol % Er^{3+}-doped hexagonal $KLaF_4$ and the digital photograph of the green glow UC are shown in the inset. (b) Log−log power dependence of the UC emissions of the hexagonal $KLaF_4$:Er^{3+} (3 mol %) sample excited at 980 nm.

SI). To ascertain whether the size of the crystallites of the products induced the phase transition on aging, the average crystallite sizes (estimated by using Scherrer analysis of their PXRD patterns) of cubic $KLaF_4$ from the reactions of $LaCl_3$, $La(acac)_3$, and $La(O^iPr)_3$ with KF at room temperature (Figure S4 in the SI) and hexagonal $KLaF_4$ from the reactions of $La(acac)_3$ and $La(O^iPr)_3$ with KF at 65 °C were compared. The average crystallite sizes of cubic $KLaF_4$ using $LaCl_3$, $La(acac)_3$, and $La(O^iPr)_3$ were 16.7, 6.3, and 2.1 nm, respectively. The average crystallite sizes of the hexagonal $KLaF_4$ samples from the reactions of $La(O^iPr)_3$ and $La(acac)_3$ with KF were 9 and 21 nm, respectively. Thus, it is evident that the crystallite sizes of cubic $KLaF_4$ using the lanthanum precursors with chelating groups are lower than the one using the lanthanum salt. Because the higher crystallite size of cubic $KLaF_4$ obtained from $LaCl_3$ did not yield hexagonal $KLaF_4$ and the smaller crystallites of cubic $KLaF_4$ [obtained from $La(acac)_3$ and $La(O^iPr)_3$ at room temperature] transformed to hexagonal $KLaF_4$ (upon aging at 65 °C), it is proposed that the average crystallite size of cubic $KLaF_4$ from these reactions is the major factor for

dx.doi.org/10.1021/ic301566e | Inorg. Chem. 2012, 51, 12748−12754

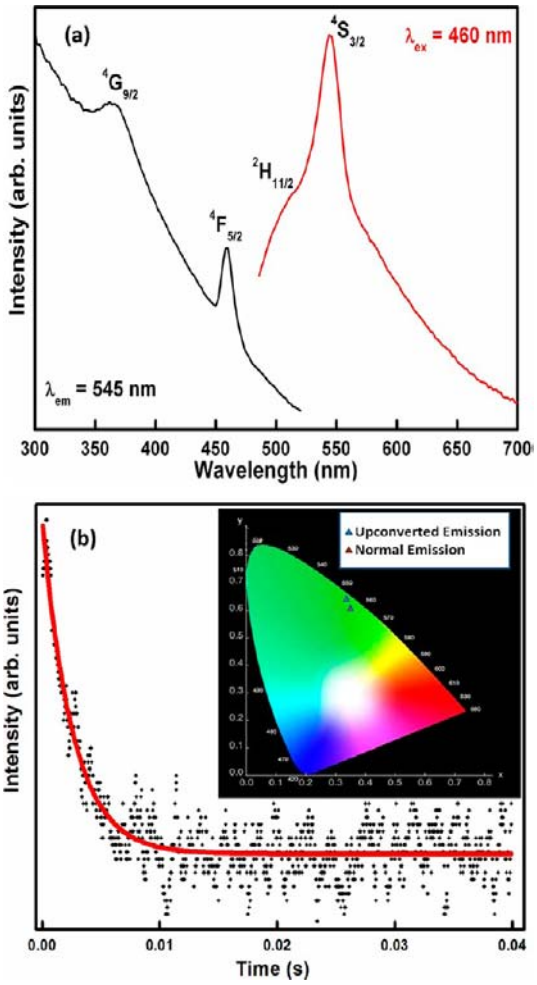

Figure 5. (a) Normal excitation (black line) and emission spectra (red line) of the 3 mol % Er^{3+}-doped hexagonal $KLaF_4$ sample. (b) UC luminescence decay curves of the $KLaF_4$:Er^{3+} (3 mol %) sample recorded with an emission of 545 nm. The inset shows a CIE (*X*, *Y*) coordinate diagram, with the chromaticity points calculated from the UC and normal emission spectra of the Er^{3+}-doped $KLaF_4$ sample.

effecting its phase transformation to hexagonal. Also, the higher average crystallite size of hexagonal $KLaF_4$ [9 and 21 nm from $La(O^iPr)_3$ and $La(acac)_3$, respectively] compared to the lower average crystallite size of cubic $KLaF_4$ [2.1 and 6.3 nm from $La(O^iPr)_3$ and $La(acac)_3$, respectively] clearly indicated that the larger crystallites have been obtained at the expense of smaller ones together with the phase transformation. Such a process has been explained through the interface nucleation mechanism for the phase transformation of colloidal In_2O_3, ZrO_2, TiO_2, and ZnS nanocrystals.[17] Also, the densely aggregated nanocrystals showed higher transformation and growth rates compared to the loosely aggregated crystals in those systems.[17] A comparison of the transmission electron microscopy (TEM) images of cubic and hexagonal $KLaF_4$ obtained from $La(acac)_3$ revealed the presence of agglomeration in both samples, suggesting that a similar mechanism might be effecting the phase transformation of the cubic $KLaF_4$ nanocrystals to the hexagonal form (Figure S5 in the SI). It can be further argued that the smaller nanocrystallites have higher packing density relative to the larger ones, might result in a higher probability of particle−particle contact formation, and thereby accelerated the phase transformation rate in $KLaF_4$. The temperature of the

Figure 6. Transparent PMMA film containing a 1 wt % hexagonal $KLaF_4$:Er^{3+} (3 mol %) film. An intense green emission upon shining with white light is shown in the inset.

reaction (65 °C) would have contributed further to the increased probability of nanocrystallites having interaction and rapid hexagonal phase nucleation. It is possible that the larger crystallites (of cubic $KLaF_4$ obtained from $LaCl_3$) might have a low particle−particle contact density, hindering interface nucleation to transform to a hexagonal polymorph and instead dissociating to LaF_3. Thus, the temperature, fluorination reaction time, nature of the lanthanum precursor, and size of the crystallites (formed initially) influenced the formation of hexagonal $KLaF_4$.

A *Diamond*[18] drawing of the hexagonally ordered $KLaF_4$ lattice is shown in Figure 1a, and the structure consists of an ordered array of F^- ions with two types of relatively low-symmetry cation sites that are selectively occupied by K^+ and La^{3+} ions. This arrangement results in significant electron cloud distortion of the cations differing from its cubic polymorph in which the high-symmetry cationic sites are randomly occupied by K^+ and La^{3+} ions.[19] It has been well documented that the transformation from cubic to hexagonal form in these fluoride systems is of a disorder-to-order character with respect to cations. Hexagonal $KLaF_4$ has been considered to be isomorphous to the β_1-K_2UF_6 structure, with the formula given as $(KLaF_4)_{1.5}$.[20] In the structural model employed for the Rietveld refinement, the site 2d was considered to be shared by 1.5 K^+ and 0.5 La^{3+} ions, while the site 1a was exclusively occupied by La^{3+} ions. Six F^- ions were equally distributed in sites 3f and 3g. Assuming spherical particles without strain, the diffractogram was well fit in the hexagonal space group $P\bar{6}2m$ (No. 189), with lattice constants of a = 6.5842(3) Å and c = 3.8165(3) Å (Figure 1b). The crystal data and structure refinement parameters of hexagonal $KLaF_4$ are summarized in Table 1. The refined unit cell and position parameters, after the final cycle of refinement, are provided in Table 2.

Hexagonal $KLaF_4$ obtained from the reaction of $La(O^iPr)_3$ and KF also showed agglomeration of crystallites in its TEM image (Figure 2a). Lattice fringes of the individual crystallites were seen in the HRTEM image, indicative of their good crystallinity (Figure 2b). The distances between the lattice

dx.doi.org/10.1021/ic301566e | *Inorg. Chem.* 2012, 51, 12748−12754

fringes were measured to be 0.33 nm, corresponding to the *d* spacing for the (110) lattice plane of the hexagonal $KLaF_4$ structure. The selected-area electron diffraction (SAED) pattern of the crystallites (inset of Figure 2b) could be indexed to the (100), (101), (200), (302), and (311) planes of the hexagonal $KLaF_4$ structure.

3.2. Optical Properties and UC Luminescence. A room temperature Raman spectrum of hexagonal $KLaF_4$ [prepared from $La(O^iPr)_3$ as the precursor] showed four phonon bands centered at 161, 231, 292, and 383 cm^{-1} (Figure 3). The effective phonon energy was calculated to be 262 cm^{-1} by the Lorentzian fitting procedure,[21] which is lower than the one reported for the widely studied $NaYF_4$ system (360 cm^{-1}).[22] Other Lorentzian fitted parameters are provided in Table S1 in the SI. Because lower phonon energies are an important aspect for minimizing nonradiative (multiphonon) losses as well as increasing the overall metastable energy lifetime of the UC processes, our estimation reinforced the superiority of $KLaF_4$ over $NaYF_4$ as the host lattice.

Doping of hexagonal $KLaF_4$ with the optically active Er^{3+} ions was examined to study its solubility and the associated optical properties including the UC. The Er^{3+}-doped (3 mol %) sample was prepared under experimental conditions identical with those employed for the undoped samples using $La(O^iPr)_3$ and KF. The close size match between the La^{3+} (La^{VI} = 1.17 Å; La^{VIII} = 1.30 Å) and Er^{3+} (Er^{VI} = 1.03 Å; Er^{VIII} = 1.14 Å) ions[23] certainly facilitated its accommodation in a hexagonally ordered fashion. Rietveld refinement of the PXRD pattern of the 3 mol % Er-doped sample is provided in Figure S6 in the SI.

The measured UV−visible diffuse-reflectance spectra in the visible and near-IR regions of the 3 mol % Er^{3+}-doped $KLaF_4$ sample are reproduced in Figure 4a. The sharp bands were assigned to the intraconfigurational f−f transitions from the $^4I_{15/2}$ ground state to the $^4I_{11/2}$, $^4I_{9/2}$, $^4F_{9/2}$, $^2H_{11/2}$, $^4F_{7/2}$, and $^4F_{5/2}$ excited states.[24] Upon excitation of the Er^{3+}-doped (3 mol %) hexagonal $KLaF_4$ sample with a 980 nm laser operating at the 150 mW power level, intense green upconverted (UC) emission with predominant emission at 545 nm along with low intense peaks at 522 and 662 nm was observed (Figure 4a). They were attributed to the transition from the $^4S_{3/2}$, $^2H_{11/2}$, and $^4F_{9/2}$ states to the $^4I_{15/2}$ ground state, respectively. The digital photograph of the intense green UC emission observed from the sample is also shown in Figure 4a in the inset. Upon comparison of the UC emission spectra of cubic $KLaF_4$:Er^{3+} with the present data, it is clear that the positions of the green and red emissions did not change with a change in the symmetry of the host lattice.[7] However, the integral luminescence intensity of the Er^{3+}-doped hexagonal $KLaF_4$ enhanced by manifolds is that of the cubic $KLaF_4$:Er^{3+} sample. The increase in the intensity could be the result of a different crystal-field environment around the Er^{3+} ions in these two host lattices. In order to determine the number of photons as well as to understand the mechanism involved in the UC process in this system, a pumping power (*P*) dependence of the intensities of the UC emission was carried out (Figure S7 in the SI). The logarithmic plots of the emission intensity as a function of the excitation power of a 980 nm laser for the emissions $^2H_{11/2} \rightarrow {}^4I_{15/2}$, $^4S_{3/2} \rightarrow {}^4I_{15/2}$, and $^4F_{9/2} \rightarrow {}^4I_{15/2}$ are shown in Figure 4b. It is very well-known that, for the UC process, the emission intensity (*I*) is proportional to P^n (where $n > 1$) for one emitted photon.[25] The plot of log *I* versus log *P* yields a straight line for the $^2H_{11/2} \rightarrow {}^4I_{15/2}$ and $^4S_{3/2} \rightarrow {}^4I_{15/2}$ transitions with slope values of *n* of 1.85 and 1.52, respectively. This implies a two-photon green (545 and 522 nm) emission process initiated at relatively low excitation powers. The slope for the red (662 nm) emission, $^4F_{9/2} \rightarrow {}^4I_{15/2}$, is 1.01, indicating that energy transfer is the dominant mechanism for the UC process.[26] Power dependencies of the UC emissions became nonlinear above 300 mW, suggesting saturation of the UC processes.[25]

The normal emission and corresponding excitation spectra for the 3 mol % Er^{3+}-doped $KLaF_4$ sample dispersed in water (~1 wt %) are shown in Figure 5a. The excitation spectrum monitored at an emission wavelength of 545 nm consisted of two broad excitation lines centered at 366 and 460 nm, which are attributed to the $^4I_{15/2} \rightarrow {}^4G_{9/2}$ and $^4I_{15/2} \rightarrow {}^4F_{5/2}$ transitions, respectively.[24] The normal emission spectrum of hexagonal $KLaF_4$:Er^{3+} excited at 460 nm followed an intense green emission similar to that of its UC emission. Two predominant peaks centered at 522 and 545 nm were observed to arise out of the transition from the $^2H_{11/2}$ and $^4S_{3/2}$ states to the $^4I_{15/2}$ ground state, respectively. The CIE1931 XY diagram of the hexagonal $KLaF_4$:Er^{3+} (3 mol %) sample is presented in the inset of Figure 5b. The calculated CIE color coordinates in UC (X = 0.355; Y = 0.623) as well in normal emission (X = 0.384; Y = 0.564) shift only slightly and fall well within the green region. The UC decay time of the $^4S_{3/2}$ state of the Er^{3+}-doped hexagonal $KLaF_4$ sample (Figure 5b) was calculated from a single-exponential fitting as 2.55 ms, suggesting minimal clustering effects.

Owing to the smaller crystallite size of the hexagonal $KLaF_4$:Er^{3+} sample, it was realized that if they are dispersed in a polymer matrix, preferably, a transparent one, it will find potential applications in three-dimensional displays and optoelectronic and radiation detectors.[27] For this purpose, 1 wt % of $KLaF_4$:Er (3 mol %) was dispersed in acetone, added to the monomer solution of methyl methacrylate (MMA) in acetone, and subjected to polymerization using a benzoyl peroxide initiator.[28] The resultant composite poly(methyl methacrylate) (PMMA) films show intense greenish color upon shining with white-light radiation (digital picture shown in Figure 6). These preliminary results are to be further explored and are quite promising toward their potential use in aforementioned objectives.

4. CONCLUSIONS

Investigations on the bulk synthesis of the hexagonally ordered $KLaF_4$ by a solution-based method revealed that both the temperature and ligands attached to the lanthanum precursor influenced its formation. While the simple lanthanum salt ($LaCl_3$) did not yield hexagonal $KLaF_4$, $La(acac)_3$ and $La(O^iPr)_3$ yielded hexagonally ordered $KLaF_4$ after aging at 65 °C for 12 h. It is reasoned out that the cubic-to-hexagonal phase transformation in $KLaF_4$, from reactions involving $La(acac)_3$ and $La(O^iPr)_3$ as the reactants, could possibly be induced by the nanosized crystallites produced in these sets of reactions via an interface nucleation mechanism. The first time synthesis of this phase facilitated its structural refinement by the Rietveld refinement procedure of its PXRD pattern. The total conservation of atoms between the reactants and the products and the nongeneration of hazardous HF during the synthesis are some of the aspects that need to be highlighted from the green chemistry point of view. Also, this method does not require a calcination step or a postannealing process. The phonon energy of this hexagonal $KLaF_4$ lattice has been determined for the first time and is lower than that of the

dx.doi.org/10.1021/ic301566e | Inorg. Chem. 2012, 51, 12748−12754

widely investigated $NaYF_4$ system. Doping of the hexagonal polymorph with optically active Er^{3+} ions illustrated its suitability as a host lattice for the energy UC process. A two-photon emission process has been demonstrated to result in the strong green UC in this system, opening a window of additional host matrices for various applications. An optically transparent thick film of PMMA containing the upconverting hexagonal $KLaF_4:Er^{3+}$ phosphor was prepared, suggesting its additional futuristic applications.

■ ASSOCIATED CONTENT

Ⓢ Supporting Information

Figures of PXRD patterns, a TG-DTA trace, TEM images, and UC emission spectra and a table of the Lorentzian peaks fitted parameters of the Raman spectrum of hexagonal $KLaF_4$. This material is available free of charge via the Internet at http://pubs.acs.org.

■ AUTHOR INFORMATION

Corresponding Author

*E-mail: rnagarajan@chemistry.du.ac.in.

Notes

The authors declare no competing financial interest.

■ ACKNOWLEDGMENTS

The authors sincerely thank and acknowledge DU-DST PURSE Grant and University of Delhi for financial support to carry out this work. The authors thank Dr. S. Uma for many useful discussions and for permitting us to use her DST-funded facilities. S.A. expresses his sincere thanks to CSIR, New Delhi, India, for the SRF fellowship.

■ REFERENCES

(1) Downing, E.; Hesselink, L.; Ralston, J.; Macfarlane, R. *Science* **1996**, *273*, 1185−1189. Hinklin, T. R.; Rand, S. C.; Laine, R. M. *Adv. Mater.* **2008**, *20*, 1270−1273. de Wild, J.; Meijerink, A.; Rath, J. K.; van Sark, W. G. J. H. M.; Schropp, R. E. I. *Energy Environ. Sci.* **2011**, *4*, 4835−4848. Trupke, T.; Shalav, A.; Richards, B. S.; Würfel, P.; Green, M. A. *Sol. Energy Mater. Sol. Cells* **2006**, *90*, 3327−3338.

(2) Rollet, A.-L.; Allix, M.; Veron, E.; Deschamps, M.; Montouillout, V.; Suchomel, M. R.; Suard, E.; Barre, M.; Ocaña, M.; Sadoc, A.; Boucher, F.; Bessada, C.; Massiot, D.; Fayon, F. *Inorg. Chem.* **2012**, *51*, 2272−2282.

(3) Chatterjee, D. K.; Rufaihah, A. J.; Zhang, Y. *Biomaterials* **2008**, *29*, 937−943. Park, Y.; Kim, J. H.; Lee, K. T.; Jeon, K.-S.; Na, H. B.; Yu, J. H.; Kim, H. M.; Lee, N.; Choi, S. H.; Baik, S.; Kim, H.; Park, S. P.; Park, B.-J.; Kim, Y. W.; Lee, S. H.; Yoon, S.-Y.; Song, I. C.; Moon, W. K.; Suh, Y. D.; Hyeon, T. *Adv. Mater.* **2009**, *21*, 4467−4471. Wang, M.; Mi, C.-C.; Wang, W.-X.; Liu, C.-H.; Wu, Y.-F.; Xu, Z.-R.; Mao, C.-B.; Xu, S.-K. *ACS Nano* **2009**, *3*, 1580−1586. Boyer, J.-C.; Cuccia, L. A.; Capobianco, J. A. *Nano Lett.* **2007**, *7*, 847−852.

(4) Wang, D.; Xie, T.; Li, Y. *Nano Res.* **2009**, *2*, 30−46. Yin, Y.; Alivisatos, A. P. *Nature* **2005**, *437*, 664−670. Murphy, C. J.; Sau, T. K.; Gole, A. M.; Orendorff, C. J.; Gao, J.; Gou, L.; Hunyadi, S. E.; Li, T. *J. Phys. Chem. B* **2005**, *109*, 13857−13870.

(5) Tyagi, A. K.; Kohler, J.; Balog, P.; Weber, J. *J. Solid State Chem.* **2005**, *178*, 2620−2625.

(6) Du, Y.-P.; Zhang, Y.-W.; Sun, L.-D.; Yan, C.-H. *Dalton Trans.* **2009**, 8574−8581.

(7) Tyagi, N.; Reddy, A. A.; Nagarajan, R. *Opt. Mater.* **2010**, *33*, 42−47.

(8) Das, S.; Reddy, A. A.; Ahmad, S.; Nagarajan, R.; Prakash, G. V. *Chem. Phys. Lett.* **2011**, *508*, 117−120.

(9) Liu, R.; Tu, D.; Liu, Y.; Zhu, H.; Li, R.; Zheng, W.; Ma, E.; Chen, X. *Nanoscale* **2012**, *4*, 4485−4491.

(10) Zachariasen, W. H. *J. Am. Chem. Soc.* **1948**, *70*, 2147−2151.

(11) Sun, Y.; Chen, Y.; Tian, L.; Yu, Y.; Kong, X.; Zhao, J.; Zhang, H. *Nanotechnology* **2007**, *18*, 275609 (1−9). Zeng., J.-H.; Su, J.; Li, Z.-H.; Yan, R.-X.; Li, Y.-D. *Adv. Mater.* **2005**, *17*, 2119−2123. Liang, X.; Wang, X.; Zhuang, J.; Peng, Q.; Li, Y. *Adv. Funct. Mater.* **2007**, *17*, 2757−2765. Wang, Z.; Tao, F.; Yao, L.; Cai, W.; Li, X. *J. Cryst. Growth* **2006**, *290*, 296−300.

(12) Ghosh, P.; Patra, A. *J. Phys. Chem. C* **2008**, *112*, 3223−3231. Yi, G.; Lu, H.; Zhao, S.; Ge, Y.; Yang, W.; Chen, D.; Guo, L.-H. *Nano Lett.* **2004**, *4*, 2191−2196.

(13) Chen, D.; Huang, P.; Yu, Y.; Huang, F.; Yang, A.; Wang, Y. *Chem. Commun.* **2011**, *47*, 5801−5803.

(14) Grzechnik, A.; Bouvier, P.; Crichton, W. A.; Farina, L.; Köhler, J. *Solid State Sci.* **2002**, *4*, 895−899.

(15) Pope, G. W.; Steinbach, J. F.; Wagner, W. F. *J. Inorg. Nucl. Chem.* **1961**, *20*, 304−313.

(16) Rietveld, H. M. *J. Appl. Crystallogr.* **1969**, *2*, 65−71. Coelho, A. A. *TOPAS*, version 3.1; Bruker AXS GmbH: Karlsruhe, Germany, 2003.

(17) Farvid, S. S.; Radovanovic, P. V. *J. Am. Chem. Soc.* **2012**, *134*, 7015−7024. Sabyrov, K.; Burrows, N. D.; Penn, R. L. *Chem. Mater.* **2012**, DOI: dx.doi.org/10.1021/cm302129a. Zhang, Y. L.; Jin, X. J.; Rong, Y. H.; Hsu, T. Y.; Jiang, D. Y.; Shi, J. L. *Mater. Sci. Eng., A* **2006**, *438−440*, 399−402. Feigl, C. A.; Barnard, A. S.; Russob, S. P. *Phys. Chem. Chem. Phys.* **2012**, *14*, 9871−9879. Huang, F.; Banfield, J. F. *J. Am. Chem. Soc.* **2005**, *127*, 4523−4529. Chraska, T.; King, A. H.; Berndt, C. C. *Mater. Sci. Eng., A* **2000**, *286*, 169−178.

(18) Brandenburg, K.; Putz, H. *Diamond*, version 3.0; Crystal Impact GbR: Bonn, Germany 2005.

(19) Wang, F.; Han, Y.; Lim, C. S.; Lu, Y.; Wang, J.; Xu, J.; Chen, H.; Zhang, C.; Hong, M.; Liu, X. *Nat. Lett.* **2010**, *463*, 1061−1065.

(20) Zachariasen, W. H. *Acta Crystallogr.* **1948**, *1*, 265−268.

(21) Sarakovskis, A.; Grube, J.; Mishnev, A.; Springis, M. *Opt. Mater.* **2009**, *31*, 1517−1524.

(22) Suyver, J. F.; Grimm, J.; van Veen, M. K.; Biner, D.; Krämer, K. W.; Güdel, H. U. *J. Lumin.* **2006**, *117*, 1−12. Shan, J.; Uddi, M.; Yao, N.; Ju, Y. *Adv. Funct. Mater.* **2010**, *20*, 3530−3537. Renero-Lecuna, C.; Martín-Rodríguez, R.; Valiente, R. *Chem. Mater.* **2011**, *23*, 3442−3448.

(23) Shannon, R. D. *Acta Crystallogr.* **1976**, *32*, 751−767.

(24) Reisfeld, R.; Jorgensen, C. K.; *Laser and Excited States of Rare Earths*; Springer-Verlag: Berlin: 1977.

(25) Pollnau, M.; Gamelin, D. R.; Lüthi, S. R.; Güdel, H. U.; Hehlen, M. P. *Phys. Rev. B: Condens. Matter* **2000**, *61*, 3337−3346.

(26) Kort, K. R.; Banerjee, S. *Inorg. Chem.* **2011**, *50*, 5539−5544. Bednarkiewicz, A.; Wawrzynczyk, D.; Gagor, A.; Kepinski, L.; Kurnatowska, M.; Krajczyk, L.; Nyk, M.; Samoc, M.; Strek, W. *Nanotechnology* **2012**, *23*, 145705. Li, Y.; Wang, G.; Pan, K.; Jiang, B.; Tian, C.; Zhou, W.; Fu, H. *J. Mater. Chem.* **2012**, *22*, 20381−20386.

(27) Li, S.; Toprak, M. S.; Jo, Y. S.; Dobson, J.; Kim, D. K.; Muhammed, M. *Adv. Mater.* **2007**, *19*, 4347−4352. Hinklin, T. R.; Rand, S. C.; Laine, R. M. *Adv. Mater.* **2008**, *20*, 1270−1273. Downing, E.; Hesselink, L.; Ralston, J.; Macfarlane, R. *Science* **1996**, *273*, 1185−1189. Godovsky, D. Y. *Adv. Polym. Sci.* **2000**, *153*, 163−205.

(28) Brydson, J. A. *Plastics Materials*; Butterworth-Heinemann: Waltham, MA, 1999.